Dyes and Pigments 156 (2018) 108–115

Contents lists available at ScienceDirect

Dyes and Pigments

journal homepage: www.elsevier.com/locate/dyepig

Diketopyrrolopyrrole pigment core@multi-layer SiO_2 shell with improved photochemical stability

Erika Švara Fabjan[a,b], Zineb Saghi[c,d,e], Paul A. Midgley[c], Mojca Otoničar[f], Goran Dražić[g], Miran Gaberšček[b,g], Andrijana Sever Škapin[a,*]

[a] Slovenian National Building and Civil Engineering Institute, Dimičeva 12, 1000 Ljubljana, Slovenia
[b] University of Ljubljana, Faculty of Chemistry and Chemical Technology, Večna pot 113, 1000 Ljubljana, Slovenia
[c] University of Cambridge, Department of Materials Science and Metallurgy, 27 Charles Babbage Road, Cambridge CB3 0FS, UK
[d] University of Grenoble Alpes, Grenoble F-38000, France
[e] CEA, LETI, MINATEC Campus, Grenoble F-38054, France
[f] Jožef Stefan Institute, Jamova cesta 39, 1000 Ljubljana, Slovenia
[g] National Institute of Chemistry, Hajdrihova 19, 1000 Ljubljana, Slovenia

ARTICLE INFO

Keywords:
Organic pigment
Silica coating
Encapsulation
Morphology
Photochemical stability

ABSTRACT

A model organic pigment (diketopyrrolopyrrole) is encapsulated by a silica coating in order to improve its photochemical stability. Unlike in previous works where single-layer silica coatings were used for similar purposes, we here propose creation of a multi-layer silica shell synthesized *via in-situ* sol-gel method, which should significantly improve the homogeneity and thus the protection ability of the coating. This is done by repeating the basic two-step process (pigment surface modification and silica encapsulation) several times, creating the final protective shell in a layer-by-layer fashion. The compositional and structural properties of the prepared coatings is studied using Fourier-transform infrared spectroscopy, differential thermal and thermogravimetric analysis, nitrogen adsorption measurements and transmission electron microscopy. Photochemical stability of non-encapsulated and encapsulated pigment particles is evaluated *via* the so-called fast-irradiation method. Various correlations between the essential coating properties, such as thickness, porosity, SiO_2 content, and the corresponding photochemical stability of the samples are established and discussed in detail. As a whole, our results confirm the basic hypothesis, that multiple-layered silica shells show improved pigment protection ability in comparison to the single-layer coatings.

1. Introduction

Organic pigments are particulate, mostly insoluble solid particles that impart colour by absorption and/or scattering of visible light. Today, they are used in many industrial and consumer sectors to satisfy aesthetic needs, to communicate, secure and protect the product [1]. The colour nuances of a pigment are determined by its molecular structure. By substitution of the coupling component, different shades of colour can be achieved [2]. Besides offering numerical colour shades, the organic pigments also exhibit poor photochemical fastness (for example when exposed UV light and TiO_2), dispersibility and resistance to heat [3,4], which results in their limited application. In an attempt to remove these limitations, different methods, mainly based on modification of the pigment particle surface, have been developed. The most frequently used approach has been encapsulation of individual pigment nanoparticles by a compact and durable shell, although a reverse silica-pigment topology has also been proposed [4]. Due to its inertness, transparency and abundance, silica seems to be a very good candidate for such a purpose. Indeed, silica has been the material of choice in many pigment encapsulation procedures and methods such as: (i) *in situ* sol-gel reaction using different silica precursors, for example a potassium/sodium silicate solution [5–7], different silanes with fumed silica [8], or tetraethoxysilane (TEOS) – probably the most popular silica precursor [9]; (ii) ball milling treatment using silica nanoparticles [10], (iii) addition of pre-synthesized silica nanoparticles using the layer-by-layer technique [11,12]. Cao et al. [13] reported on fabrication of inorganic-organic hybrid pigments by adding an inorganic mixture of precipitated SiO_2 and TiO_2. Another way to produce a dye core@silica shell structure is *via* the mesoporous soft templated synthesis [14]. In order to improve the interactions between the surface

* Corresponding author. Slovenian National Building and Civil Engineering Institute, Dimičeva 12, 1000 Ljubljana, Slovenia.
E-mail addresses: erika.svara-fabjan@zag.si (E.Š. Fabjan), zineb.saghi@cea.fr (Z. Saghi), pam33@cam.ac.uk (P.A. Midgley), mojca.otonicar@ijs.si (M. Otoničar), goran.drazic@ki.si (G. Dražić), miran.gaberscek@ki.si (M. Gaberšček), andrijana.skapin@zag.si (A.S. Škapin).

https://doi.org/10.1016/j.dyepig.2018.03.064
Received 16 January 2018; Received in revised form 27 March 2018; Accepted 28 March 2018
Available online 29 March 2018

of the pigment and the silica, the former has often been pre-modified using different polyelectrolytes [12] and surfactants [7].

In our previous work [7] we used the two-step silica encapsulation approach to protect the surface of a model pigment – diketopyrrolopyrrole. In the first step the surface of the pigment was modified by a mixture of ionic and non-ionic surfactants (forming the so-called mixed micelle system), whereas in the second step a silica shell was formed using a sol-gel reaction with potassium silicate solution ($K_2O \times 3.9SiO_2$) as a silica precursor. We found that the dispersion properties of the organic pigment particles depended on the surface properties of the core material (organic pigment particles) so an appropriate modifier was chosen to tune those properties [7]. Furthermore, experiments showed that the growth of a continuous silica shell was promoted by an appropriate mixture of ionic and non-ionic surfactant, which helped reduce the electrostatic repulsion between the cationic head groups. The thickness of the shell could be altered by the synthesis temperature – the higher the temperature, the thicker was the shell. Despite succeeding to prepare a rather uniform, continuous silica shell, the pigment protection against photocatalysis (exposure to UV light at 180 W m^{-2}) was only up to 27% better than in the reference pigment without silica shell, which was rather unexpected. Furthermore, whereas by raising the synthesis temperature from 70 °C to 90 °C the average shell thickness expectedly increased (from 3-4 nm to 10–12 nm), the protection ability surprisingly decreased. This was explained by a decrease of shell homogeneity, i.e., by the occurrence of large defects in shells at higher temperatures. Even more intriguing observations were reported by Velho et al. [15], who studied the encapsulation of natural dyes using a TEOS as a silica precursor; stating that after encapsulation, the protection against UV radiation was even decreased.

In order to address the problem of insufficient shell homogeneity and, consequently, its rather low protection ability, we here propose formation of a multi-layer silica shell synthesized *via* an *in situ* sol-gel method rather than using already pre-synthesized silica nanoparticles – a route commonly found in the literature [11,12]. The main approach consists of repeating the basic two-step process (pigment surface modification and silica encapsulation) several times, i.e. creating the final protective shell in a layer-by-layer fashion. As in the previous paper [7], a mixture of surfactants is used, whereas the silica encapsulation step is carried out by an *in situ* sol-gel synthesis using potassium silicate as a silica precursor. In the previous paper only one step and consequently one layer of shell was synthesized and studied [7], whereas in this paper creation and evaluation of a multilayer shell is the main topic. The correlations among the number of multilayer encapsulation, the amount of SiO_2 in the sample, shell thickness, shell porosity and its photochemical stability were studied in detail. The synthesized materials are characterized in great detail using transmission electron microscopy (TEM), scanning transmission electron microscopy (STEM), energy-filtered transmission electron microscopy (EF-TEM), Fourier transform-infrared (FTIR) spectroscopy and thermogravimetric analyses.

2. Materials and methods

2.1. Materials

The red pigment 3,6-bis(4-chlorophenyl)pyrrolo[3,4-*c*]pyrrole-1,4-dione (*p*-Cl-DPP), also known as C.I. Pigment Red 254, was provided by Clariant, Switzerland (the structural formula is presented in Fig. 1a and the morphology in the TEM micrograph in Fig. 1b). As shown in our previous report the pigment is crystalline, corresponds to α-polymorphic modification. According to the manufacturer, it does not contain any significant impurities [7]. Hexadecyl-trimethylammonium bromide (CTAB), hydrochloric acid, butan-1-ol and ethanol were obtained from Sigma Aldrich, Germany. Ethoxylated alcohol $C_{12}/C_{13}(OC_2H_4)_5H$ (EA) was purchased from Air Products&Chemicals, US

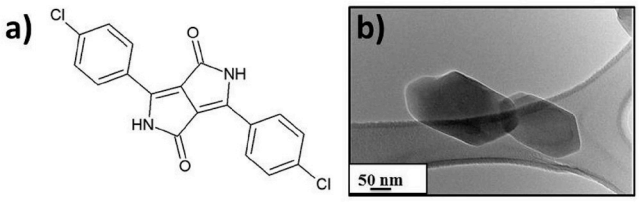

Fig. 1. a) Shematic presentation of the structural formula of *p*-Cl-DPP; b) TEM micrograph of a typical *p*-Cl-DPP particle (the neat pigment particle) such as used in this paper. In continuation this sample is labelled as »NE« (non-encapsulated).

(available on the market as Tomadol 23–5). Titanium dioxide (P25) was obtained from Evonik, Germany and solution of potassium silicate – water glass ($K_2O \times 3.9SiO_2$ – solid content 28.6 wt%) from Woellner, Germany. SiO_2 nanoparticles (Silica gel 60) used as standard for FTIR analysis were obtained from Sigma Aldrich.

2.2. Syntheses

Core@shell pigment-multi-layer SiO_2 composites were synthesized in the following way. The solution of surfactant was prepared by addition of appropriate amount of CTAB and EA, 0.025 wt% and 0.00625 wt%, respectively, into distilled water. An adequate amount of the *p*-Cl-DPP pigment was added to the solution of surfactants to obtain a 1 wt% pigment dispersion. The criteria for selection of optimal surfactant mixtures to obtain target surface properties of the *p*-Cl-DPP pigment were described in detail in our previous work [7].

2.2.1. Single-layer encapsulation

The detailed procedure for preparation of a single-layer of silica shell around organic pigment particles is described in our previous work [7]. In the current work this procedure was repeated to create multilayer encapsulations. Briefly, the shell was formed using an *in situ* sol-gel procedure wherein the dispersion of surface modified pigment particles was heated to a target temperature 70 °C while simultaneously adding potassium silicate as a silica precursor and hydrochloric acid as a pH regulator. Three different concentrations of the silica precursor water glass were used, so that the corresponding ratios between SiO_2 and the pigment in dispersions were: 0.1:1; 0.2:1 and 0.4:1 (see Table 1 – column entitled Ratio between SiO_2 and the pigment for individual encapsulation). An appropriate amount of 0.1 M HCl was added to the dispersions to keep the pH value at 8. After stirring at the target temperature for 30 min the dispersion was filtered and the deposit washed.

Table 1
Sample labels of non-encapsulated and encapsulated pigment particles.

Sample label	Ratio between SiO_2 and the pigment for individual encapsulation	Syntheses repeated (n - times)	Calcined
NE	0	0	No
E-01-1	0.1:1	1	No
E-01-2	0.1:1	2	No
E-01-3	0.1:1	3	No
E-02-1	0.2:1	1	No
E-02-2	0.2:1	2	No
E-02-3	0.2:1	3	No
E-04-1	0.4:1	1	No
E-04-2	0.4:1	2	No
E-04-3	0.4:1	3	No
EC-04-1	0.4:1	1	Yes
EC-04-2	0.4:1	2	Yes
EC-04-3	0.4:1	3	Yes
SiO_2	/	/	/

Note: NE refers to non-encapsulated pigment particles - the neat pigment particles.

2.2.2. Double-layer encapsulation

To obtain a "double-layer" silica shell, the filtrate obtained after the single-layer encapsulation was first redispersed in a mixture of CTAB and EA to again obtain the target 0.025 wt% and 0.00625 wt% dispersions, as described in the procedure above. Then the sol-gel synthesis was repeated exactly in the same way as described in the case of single-layer encapsulation - to obtain the "double-layer encapsulated" particles.

2.2.3. Triple-layer encapsulation

Both the redispersion of filtrate and the silica encapsulation procedure were repeated in the same way as described under subchapter Double-layer encapsulation – to obtain the "triple-layer encapsulated" pigment particles.

2.2.4. Calcination

In order to remove the organic matter (i.e., "cores" of the core-shell composite particles), the silica encapsulated pigment particles were heated up to 600 °C for 1 h. In this way, the pigment core was burn away and samples of calcined silica shells were obtained.

2.3. Characterization

Fourier-transform infrared spectroscopy (FTIR) was performed using a Perkin Elmer Spectrum 100 spectrometer. Approximately 2 mg of the sample was mixed with 120 mg of KBr and compressed at 10,000 kg to form a tablet with a diameter of 0.8 cm.

The morphological properties of encapsulated pigment particles were characterized using two transmission electron microscopes (TEM), a Jeol JEM-2100 and an ARM 200 CF (Jeol Ltd., Tokyo, Japan) both operated at 200 kV. The ARM 200 CF was used to record scanning transmission electron microscope (STEM) images in the high-angle annular dark field (HAADF) mode. The samples were dispersed in water or ethanol and filtered through a 100-mesh copper grid. The SiO_2 shell thickness was systematically determined from TEM micrographs. Due to better contrast and visibility, only calcined samples were analysed. Although the pigment voids seem to collapse slightly after the pigment removal, the shell thicknesses of as-synthesized encapsulated samples and their calcined analogues are comparable. For each sample three different micrographs were collected and the shell thicknesses were measured at 12 different areas. The measurement of the shell thicknesses were performed only at the smooth – continuous part of the shells (the silica particles bonded on the surface of the shells were not considered in the measurements). The displayed d_{SiO2} values are the average values of those 12 measurements. Electron tomography was performed on a FEI Tecnai F20, field-emission gun TEM operated at 200 kV. Energy filtered TEM (EFTEM) mode was chosen to generate elemental distribution images with the "three-window method". The sample was tilted between −45deg and +60deg with 5deg increment, and at each tilt three images were taken around the C K-edge (284 eV) and Si $L_{2,3}$-edge (99 eV) respectively. Digital Micrograph was used to generate the elemental tilt series which were then transferred to Inspect3D for the alignment and reconstruction.

Nitrogen-adsorption measurements were performed at 77 K using an ASAP 2020 analyzer. The specific surface and pore size distribution were determined using the BET (Brunauer, Emmet and Teller) method and the BJH (Barrett, Joyner and Halenda) method, respectively.

Differential thermal and thermogravimetric analysis were performed using a STA 409 PC Luxx thermal analyzer, Netzsch, Germany. The samples were heated from 25 to 1400 °C in the atmosphere of synthetic air. Approximately 30 mg of the sample was analysed using the standard Pt crucibles. The parts of weight of SiO_2 in the samples (wt_{SiO2}) were determined as weight loss of the samples at 600 °C.

Photochemical stability (PS) of non-encapsulated and encapsulated pigment particles was evaluated *via* the fast-irradiation method, as presented in detail elsewhere [5,6].

The dried mixture of TiO_2 photocatalyst P25 and the pristine pigment particles in a mass ratio 5:1. was exposed to UV light (Metal halide lamp, 60 W m^{-2}) for up to 72 h. In a previous study two different UV light intensities were used, i.e., 60 and 180 W m^{-2}. In this paper we decided to only use the former conditions (60 W m^{-2}) because this value corresponds much better to the natural UV intensity. Before and after the UV exposure a colorimeter i1(X-Rite, USA) was used to evaluate the colour of the samples, using the CIE 1976 (L^*, a^*, b^*) colour space (CIELAB). Additionally, chromaticity (c^*) of CIE Lch colour space was measured on unexposed samples of encapsulated and pristine pigment particles mixed with TiO_2. The total colour change (ΔE^*) was calculated from the CIELab measurements, performed before and after UV irradiation, using the following equation:

$$\Delta E^* = \sqrt{(\Delta a^{*2} + \Delta b^{*2} + \Delta L^{*2})} \quad (1)$$

The efficiency of the shell to protect the organic pigment particles against highly reactive species was evaluated through comparison of the total colour change before and after UV irradiation. More specifically, the so-called photocatalysis protection or photochemical stability (PS) was calculated using the following equation:

$$PS = \frac{\Delta E^*_{ES} - \Delta E^*_{NE}}{\Delta E^*_{NE}} \quad (2)$$

where ΔE^*_{ES} and ΔE^*_{NE} represent the total colour change for encapsulated and non-encapsulated pigment particles, respectively.

3. Results and discussion

3.1. Comparison of the properties of the encapsulated pigments' particles after single and multi-layer shell synthesis

3.1.1. Morphological properties

The basic properties of organic pigment particles encapsulated by a single layer silica shell were presented in detail in our previous work [7]. In this article the same encapsulation procedure was used, i.e. *in situ* sol-gel reaction with potassium silicate as a silica precursor however, it was repeated several times to obtain a multi-layer shell (the single layer encapsulation was here included merely for the sake of direct and credible evaluation of the effect of multiple layer encapsulation). The final goal was to improve the silica shell homogeneity and, consequently, to increase the efficiency of pigment protection against external agents – specifically UV irradiation.

The development of morphological features of the pigment-silica system upon progressive addition of silica layers can be seen in Fig. 2. In the case of a single-layer shell (Fig. 2a), the pigment particles were covered by a thin shell, continuously spread across the surface of the pigment core with a few nanoparticles bonded onto the surface of the shell. In this case the shell thickness (d_{SiO2}) was found to be between 3 nm and 4 nm and is only slightly affected by the precursor concentration, consistently with the previous report [7].

Intuitively, double (Fig. 2b) and triple (Fig. 2c) encapsulated pigment particles are expected to possess double or triple silica shells, i.e. each encapsulation step is supposed to create one shell. Indeed, a careful study of the micrographs taken after calcination (Fig. 2d, 2e, 2f) shows that the shells get thicker after multiple deposition of silica shell. The estimated shell thicknesses (d_{SiO2}) for double and triple encapsulation are 5–9 nm and 7–13 nm, respectively. In both cases the lowest and the highest interval values correspond consistently to the lowest and the highest precursor concentrations used.

3.1.2. Confirmation of the presence of SiO_2 in the samples

FTIR spectroscopy was used to confirm the presence of SiO_2 in the samples of encapsulated pigment particles (Fig. 3). Spectra of non-encapsulated pigment particles (sample NE) were compared to the spectra of pigment particles having a single or multi-layer silica shell (samples

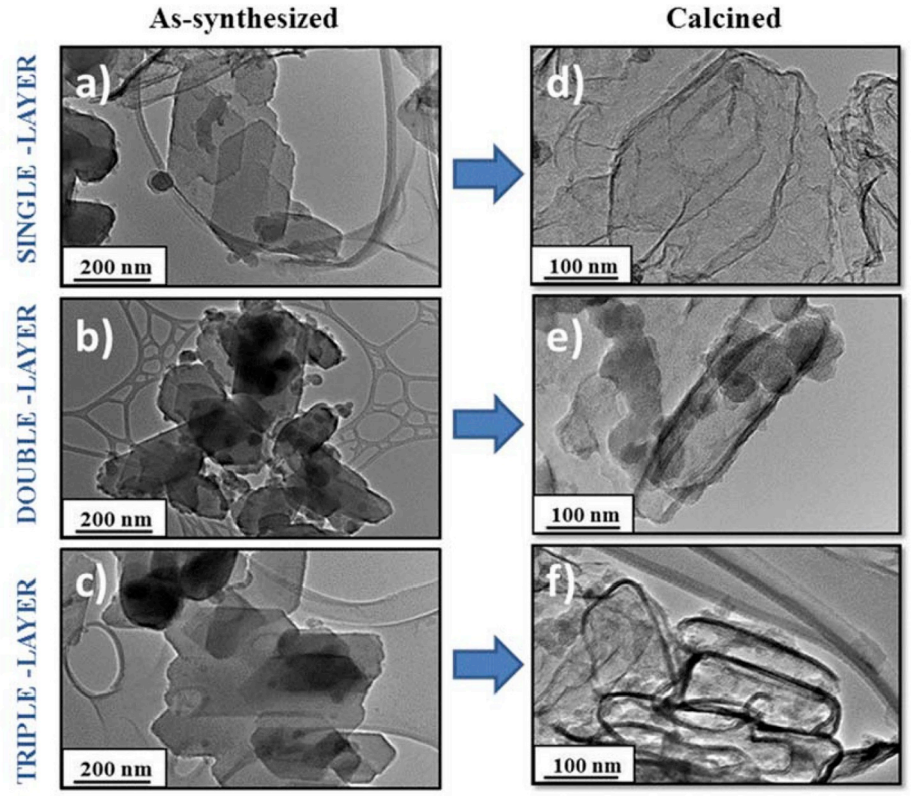

Fig. 2. TEM micrographs of as-synthesized encapsulated pigment particles: a) E-04-1, b) E-04-2 and c) E-04-1, and micrographs of the shells obtained after calcination: d) EC-04-1, e) EC-04-2 and f) EC-04-3.

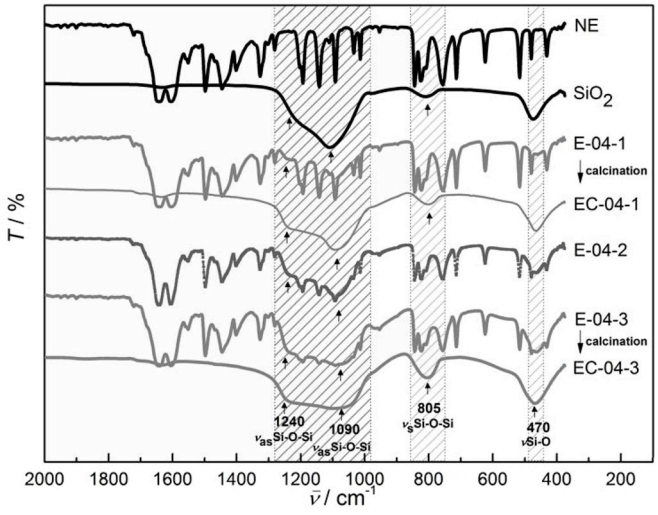

Fig. 3. FTIR spectra of SiO_2 gained on the market and following samples: non-encapsulated (NE), single-layer encapsulated (as-synthesized, E-04-1, and calcined, EC-04-1), double-layer encapsulated (E-04-2) and triple-layer encapsulated (as-synthesized, E-04-3, and calcined, EC-04-3) pigment particles.

E-04-1, E-04-2 and E-04-3) as well as to selected calcined samples (EC-04-1 and EC-04-3). As a reference material, pure SiO_2 nanoparticles available on the market (sample SiO_2) were also investigated with FTIR spectroscopy. The latter (Fig. 3, spectrum SiO_2) shows three absorption bands: at around 1090 (with the shoulder at 1240 cm^{-1}), 805 and 470 cm^{-1}. All are characteristic bands of silicon dioxide - the first two correspond to Si-O asymmetric and symmetric stretching motions, respectively, whereas the latter (at 470 cm^{-1}) belongs to a bending Si-O-Si mode [16]. FTIR spectra of non-encapsulated pigment particles as well as the encapsulated ones show several bands (Fig. 3 - spectra NE, E-04-1, E-04-2 and E-04-3) in the range from 400 to 1800 cm^{-1}. In order to make the analysis clearer, we also measured FTIR spectra of selected samples after calcination (see experimental section, subsection 2.2.4 Calcination) which was supposed to remove all the organic matter. In both cases (samples EC-04-1 and EC-04-3) all three absorption bands characteristic for SiO_2 vibrations were clearly identified (see Fig. 3, shaded areas). The changes in SiO_2 vibration modes after calcination are marked with arrows.

3.1.3. Photochemical stability

The photochemical stability (PS) was evaluated *via* a fast irradiation method using the total colour change/colour difference, ΔE^*, of samples after UV irradiation, as described in our previous papers [5,6]. A mixture of TiO_2 and non-encapsulated or encapsulated pigment particles was monitored as a function of exposure time to a UV irradiation (Fig. 4). A lower value of ΔE^* means a better PS and vice versa. For easier comparison, the main trends are shown in a single graph (Fig. 4a) where the results of double-layer shells are omitted due to their overlapping with the single-layered shells. Several conclusions seem straightforward: i) any silica treatment improves the photochemical stability of organic pigment (compare coloured curves with the black one); (ii) in all cases the triple-layer shell (dotted lines) provides a better photochemical stability than the single-layer shell (solid lines); (iii) within the same set (single or triple-layer) a higher precursor concentration leads to a better stability (compare blue, yellow and green graphs within solid or dotted lines); (iv) accordingly, the best protection is achieved by the triple-layer shell with the highest precursor concentration for which the change of ΔE^* after 72 h is about 23; this is almost twice less than in non-encapsulated pigment (ΔE^*_{NE} is approximately 40).

The more detailed results shown in Fig. 4b–d reveal that the single- and double-layer shells provide a similar pigment protection level

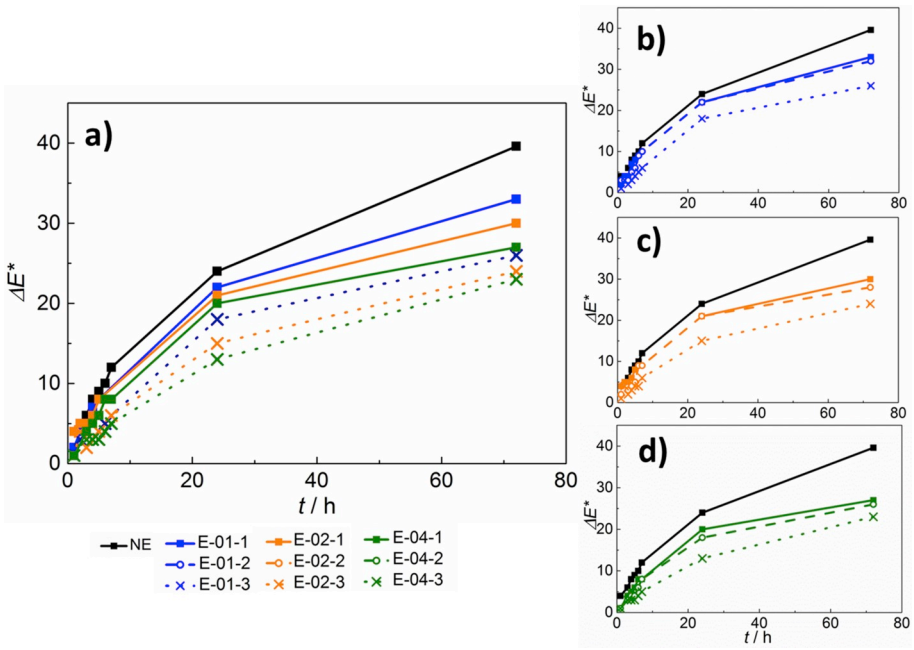

Fig. 4. Evaluation of photochemical stability in terms of protection against photocatalysis using the total colour change/colour difference, ΔE^*, of samples after UV irradiation: a) NE, single and triple-layer encapsulated pigment particles with variable precursor concentration, b) NE, E-01-1, E-01-2, E-01-3; c) NE, E-02-1, E-02-2, E-0-3; d) NE, E-04-1, E-04-2, E-04-3. (For interpretation of the references to colour in this figure legend, the reader is referred to the Web version of this article.)

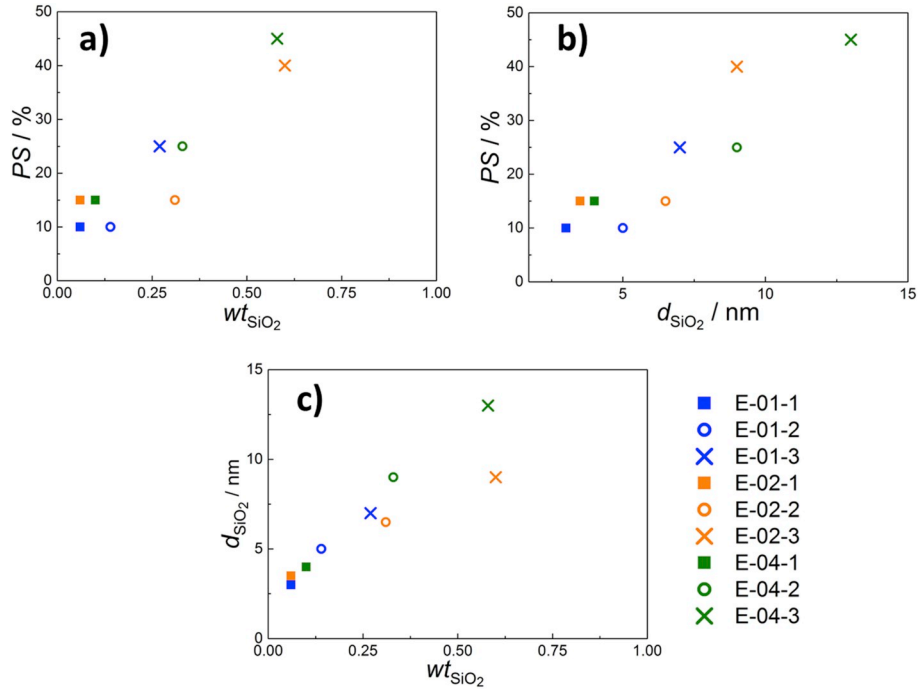

Fig. 5. Dependence of photochemical stability (PS) after 24 h of UV exposure on: a) parts by weight of SiO_2 (wt_{SiO2}) in the sample as determined using weight loss by thermogravimetry, (b) shell thickness (d_{SiO2}) estimated by TEM and c) relationship between silica shell thickness and wt_{SiO2}.

(compare solid and dashed lines). This result is rather difficult to explain if the protection ability is correlated to the parts of weight of SiO_2 in the samples (wt_{SiO2}) as determined by thermal analysis and/or the shell thickness (d_{SiO2}) only (see Table S1). It should be noted that the silica particles bonded on the surface of the shells due to secondary nucleation were not considered in the measurements of the shell thickness. Namely, according to Fig. 5a and b and Table S1, significantly thicker shells and higher wt_{SiO2} were found for the double encapsulation procedure (see double encapsulated samples E-01-2, E-02-2 and E-04-2, denoted with open circles in Fig. 5a and b). Whereas the thicker shell and the higher amount of SiO_2 in double-coated samples do not result in better PS - with respect to the single-coated pigments, the triple-encapsulated samples do exhibit the expected increase in PS. However, for the maximum precursor concentration (green points in Fig. 5c) the increase in shell thickness is much more rapid and becomes more or less linearly dependent on the wt% of silica in a sample. Although the silica particles bonded on the surface of the shells were not taken into account we estimate that they have a negligible effect on findings described in this paper.

The main trends presented above can be explained as follows. (i) We assume that the silica growth from the more concentrated dispersions results in a more porous shells. (ii) Furthermore, based on the previous report [7], we hypothesize that defects in the shell play an even more important role in protection ability than the thickness itself. In order to

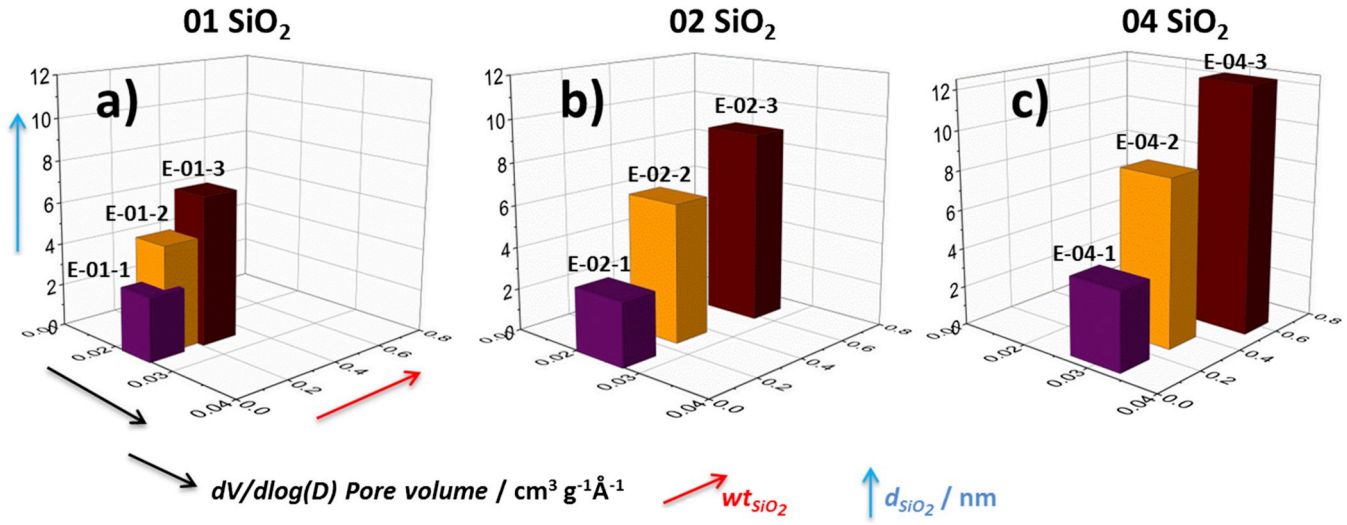

Fig. 6. Interdependence of silica thickness, d_{SiO2}, (z-axis), its porosity, *dV/Dlog(D) pore volume*, (x-axis) and its part by weight in the pigment-silica composite, wt_{SiO2}, (y-axis) at three different silica precursor concentrations: a) 0.1 g of SiO_2 per 1 g of pigment, b) 0.2 g of SiO_2 per 1 g of pigment and c) 0.4 SiO_2 per 1 g of pigment. The different column colours designate the number of encapsulations: violet, orange and brown stand for single, double and triple encapsulation procedures, respectively. (For interpretation of the references to colour in this figure legend, the reader is referred to the Web version of this article.)

get further insight into this interplay, additional morphological features of the prepared shells were investigated.

One such feature is the volume of pores and pore-size distribution within the shells. In most cases the open pore size distribution determined by the BJH method was found to be unimodal – a broad peak between approximately 20 and 80 nm could be observed (see Fig. S1 in Supplementary data). The exceptions were the triple encapsulated pigment particles which showed an additional broad peak around 10 nm. The maximum value of the volume of the pores in the range between 2 and 5 nm was found negligible for all the samples. For example, the maximum pore volumes in the range 2–5 nm for E-01-3 and E-04-3 were 0.03 $cm^3 g^{-1} Å^{-1}$ and 0.05 $cm^3 g^{-1} Å^{-1}$, respectively (see pore size distribution from BJH method in Supplementary data, Figs. S1 and S2).

The effects of silica precursor concentration on three essential shell properties, i.e. its thickness (d_{SiO2}), porosity (*dV/dlog(D) pore volume*) and the content of SiO_2 (in terms of weight fraction, wt_{SiO2}) in the pigment-silica composite were studied in more detail. Their inter-dependence is presented in Fig. 6. Clearly, when going from the lowest to highest precursor concentration (from Fig. 6a–c) the shell thickness is significantly increased – that is, the columns get significantly higher. In contrast, an increase in precursor concentration from the intermediate to highest value does not increase significantly the content of SiO_2 (compare the wt_{SiO2} axis for Fig. 6b and c where the values remain more or less constant). As the thickness of shell is increasing by increasing precursor concentration (see Fig. 5c), this could mean that the average porosity is also simultaneously increasing when going from Fig. 6b to c. This assumption, however, appears counterintuitive as one naturally expects that by the repetitive deposition of silica the eventual pores will be more and more closed, i.e. the shell will be more and more compact.

Note, however, that the differential pore volume evaluation in Fig. 6 is restricted to the smallest pores of several nanometer in diameter (specifically in the range from 2–5 nm). This parameter tells little about the much larger defects or morphological inhomogeneities which might explain some of the unexpected results shown in Fig. 6. In order to further clarify these seemingly controversial results we performed a detailed microscopical analysis of selected samples, as shown in the following section.

The colour properties of pure pigment were evaluated *via* the measurement of chromaticity (c^*) of pigment particles, mixed with TiO_2. It was found that after single or after multilayer encapsulation the chromaticity decreased only slightly (Table S1). For example, the chromaticity of non-encapsulated pigment particles was about 52 (NE in Table S1), whereas the values for various encapsulated pigment particles were between 44 and 48.

3.2. Detailed morphological properties of triple encapsulated pigment particles

The triple-encapsulated organic pigment particles, which showed the most promising results according to the photochemical stability testing, were additionally characterized using EFTEM tomography and HAADF STEM microscopy.

Electron tomography in the EFTEM mode was used to produce elemental mapping in 3D view in order to define the coverage quality of the silicon shells on the pigment particles. In comparison with the HAADF imaging, which gives more detailed information on the elemental distribution by Z-contrast, electron tomography is a more suitable method as it enables producing cross-section views of particles, reducing the overlapping of the detected elements.

Fig. 7a shows a BF-TEM image of the region selected for EFTEM tomography. The elemental distribution maps of Si and C at 0° are shown in Fig. 7b, highlighting the core-shell structure of the particle. The 3D reconstructions in Fig. 8 show the uniformity of the core and the shell.

Detailed investigation of triple encapsulated pigment particles (sample E-04-3) using HAADF-STEM imaging method revealed important differences in the image contrast of different parts of encapsulated pigment particles (Fig. 9), which most likely reflects the presence of elements with different Z number and/or different thickness. Taking a closer look to the outer part of the encapsulated pigment particles (Fig. 9b), one can observe darker spots of globular shapes and a size around 3.5 nm inside particles (see Fig. 9b marked with arrows), which suggests the presence of mesopores in the pigment shell.

To further confirm/refute the presence of mesoporous structure in the silica shell, selected samples were re-investigated using the BJH method. Again, as a reference sample the non-encapsulated pigment was used. The sample chosen was the as-synthesized triple encapsulated pigment (sample E-04-3), for which we assumed that pores could still be partially filled with surfactants. For comparison, a calcined sample (EC-04-3) was also investigated where all the surfactant was supposed to be removed. For both the non-encapsulated as well as encapsulated

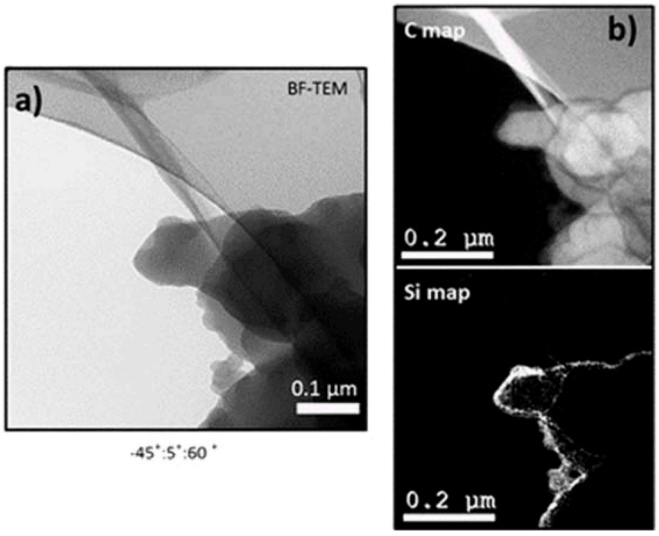

Fig. 7. a) 0deg Bright-Field TEM image of the particle selected for EFTEM tomography (−45:5:60); b) C and Si elemental distribution maps at 0deg highlighting the core-shell structure of the particle.

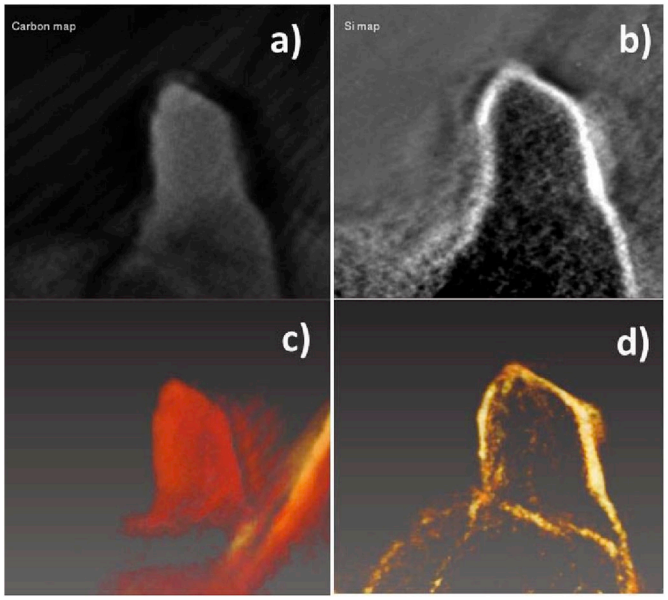

Fig. 8. EFTEM reconstruction: a) and b) x-y cross-section through the reconstructed Si and C elemental volumes; c) and d) voxel rendering of the 3D C core and Si shell, respectively.

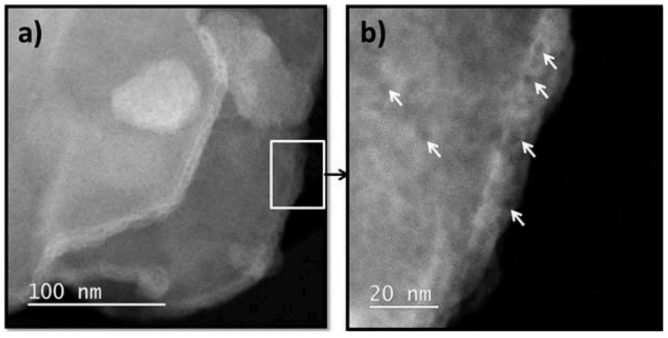

Fig. 9. HAADF- STEM micrographs of the E-04-3 sample; a) micrograph at lower magnification and b) inset of marked area in a). Arrows point out the pores in the silicon layer.

pigment particles, the pore size distributions are mainly unimodal, showing a broad peak between approximately 10–100 nm (Fig. S2 - Supplementary data). Since from the TEM micrographs it can be clearly observed that the non-encapsulated pigment particles (the neat pigment particle) are not porous (Fig. 1b), we assumed that the peak corresponded to the voids formed between the particles (i.e. to the so-called interparticle porosity). The same assumption is proposed also for encapsulated/calcined pigment particles. The same phenonomenon was observed also for the phthalocyanine pigments and was presented in one of our previous works [6]. The volumes of pores with a diameter of 2–5 nm are negligible (see the inset in Fig. S2 of the Supplementary data). Additionally, it should be noted that determination of the pore size distribution using the BJH method. The assumption that the pores are either cylindrical or slit-shaped. Taking into account these facts and our observations, one may suggest that the darker parts observed using STEM analysis could represent (1) pores that are not available to the external fluid, i.e. they are closed, (2) open pores of poorly-defined shapes that are not accessible to the BJH method.

These findings can additionally explain the non-linear correlation between the SiO_2 weight part (wt_{SiO_2}) in composite samples and the shell thickness (Fig. 5c) as well as the limited photochemical stability even in the case of triple encapsulation. Both phenomena are ascribed to a greater porosity of the samples that are grown from dispersions with a higher concentration of silica. Thus even if a greater concentration of silica in dispersion results in a higher nominal thickness of the silica shell, the protection ability increases less than expected due to the higher porosity of such thicker shells. On the other hand, the multiple encapsulation procedure does help to cover larger defects, which is probably the reason for the considerable increase of PS in multi-layered pigment particles regardless of the silica concentration in dispersion (see Figs. 5 and 6).

4. Conclusion

The surface of the diketopyrrolopyrrole pigment cores was successfully covered by silica shells with different thicknesses using *in situ* sol-gel chemistry. The shell thickness was controlled in two ways: (1) by changing the precursor concentration and (2) by repetitive deposition of “single” silica layer. Already in the case of a single-layer deposition, the silica shell was shown to have quite uniform thickness of several (3–4) nanometres, which had a measurable effect on the protection of the pigment. Expectedly, with the increasing number of silica depositions the silica shell thickness increased (up to 7–13 nm for triple shells). Consistently, photochemical stability of the pigment also increased by a similar factor. Similarly, the increase in concentration of the silica precursor also led to thicker and more protective coatings. However, we observed that when using higher silica precursor concentrations, the corresponding films developed considerable porosity, which, partly, had a negative influence on the pigment protection ability. In short, it seems that in order to increase the pigment stability, preparation of multiple silica coatings is a more efficient strategy than increasing the concentration of the silica precursor. Still, the highest pigment protection ability was achieved when using both approaches simultaneously: the so-called photochemical stability (PS) was increased by about 45% with respect to unprotected samples.

Acknowledgments

We acknowledge financial support from the Slovenian Research Agency through the research programme No. P2-0273 and post-doctoral project No. Z1-8149.

Appendix A. Supplementary data

Supplementary data related to this article can be found at https://doi.org/10.1016/j.dyepig.2018.03.064.

References

[1] Hao ZM, Iqbal A. Some aspects of organic pigments. Chem Soc Rev 1997;26:203–13.
[2] Herbst W, Hunger K. Industrial organic pigments. Weinheim: Wiley-VCH Verlag GmbH & Co; 2004. KGaA.
[3] Abel A. Paint and Surface Coatings. second ed. Lambourne: Woodhead Publishing; 1999.
[4] Fei XN, Zhang TY, Zhou CL. Modification study involving a Naphthol as red pigment. Dyes Pigments 2000;44:75–80.
[5] Thomas Rees C. Encapsulation of organic pigments. 1974. U.S. Patent 3,826,670, ZDA.
[6] Svara Fabjan E, Sever Skapin A, Skrlep L, Zivec P, Ceh M, Gaberscek M. Protection of organic pigments against photocatalysis by encapsulation. J Sol Gel Sci Technol 2012;62:65–74.
[7] Svara Fabjan E, Otonicar M, Gaberscek M, Sever Skapin A. Surface protection of an organic pigment based on a modification using a mixed-micelle system. Dyes Pigments 2016;127:100–9.
[8] Fei XN, Cao LY, Liu YL. Modified CI Pigment Red 170 with a core-shell structure: preparation, characterization and computational study. Dyes Pigments 2016;125:192–200.
[9] Yuan JJ, Zhou SX, Gu G, Wu LM. Encapsulation of organic pigment particles with silica via sol-gel process. J Sol Gel Sci Technol 2005;36:265–74.
[10] Horiuchi S, Horie S, Ichimura K. Core-shell structures of silica-organic pigment nanohybrids visualized by electron spectroscopic imaging. ACS Appl Mater Interfaces 2009;1:977–81.
[11] Yuan JJ, Zhou SX, You B, Wu LM. Organic pigment particles coated with colloidal nano-silica particles via layer-by-layer assembly. Chem Mater 2005;17:3587–94.
[12] Yuan JJ, Xing WT, Gun GX, Wu LM. The properties of organic pigment encapsulated with nano-silica via layer-by-layer assembly technique. Dyes Pigments 2008;76:463–9.
[13] Cao LY, Fei XN, Zhao HB, Gu YC. Inorganic-organic hybrid pigment fabricated in the preparation process of organic pigment: preparation and characterization. Dyes Pigments 2015;119:75–83.
[14] Bongur R, Le Nouen D, Gaslain F, Marichal C, Lebeau B, Guarilloff P. Red 33 dye co-encapsulated with cetyltrimethylammonium in mesoporous silica materials. Dyes Pigments 2016;127:1–8.
[15] Velho SRK, Brum LFW, Petter CO, dos Santos JHZ, Simunic S, Kappa WH. Development of structured natural dyes for use into plastics. Dyes Pigments 2017;136:248–54.
[16] Duran A, Serna C, Fornes V, Navarro JMF. Structural considerations about SiO2 glasses prepared by sol-gel. J Non-Cryst Solids 1986;82:69–77.